Trajectory and wake differences between disks and square plates

Luis Blay Esteban

Faculty of Engineering and the Environment
University of Southampton
SO17 1BJ, Southampton, Hampshire, UK
lbe1g14@soton.ac.uk

John Shrimpton

Faculty of Engineering and the Environment
University of Southampton
SO17 1BJ, Southampton, Hampshire, UK
J.Shrimpton@soton.ac.uk

Bharathram Ganapathisubramani

Faculty of Engineering and the Environment
University of Southampton
SO17 1BJ, Southampton, Hampshire, UK
G.Bharath@soton.ac.uk

7D-1

ABSTRACT

The free fall motion of a thin disk with small dimensionless moment of inertia was investigated experimentally and compared with the motion of a thin square plate. Both thin particles share the same frontal area but have a significant difference in the dimensionless moment of inertia, being $I^* \approx 5 \cdot 10^{-3}$ for the disk and $I^* \approx 1.7 \cdot 10^{-3}$ for the square plate. The disk trajectory is characterised by a quasi-2D oscillatory motion, while the square plate trajectory shows severe 3D motion. The wake characteristics of these particles is investigated by means of three-dimensional measurements of the instantaneous velocity field (V3V). The wake behind free falling disks is shown to be as a succession of hairpin vortices shed off at every turning point linked by means of a pair of counter rotating vortices that grow from the leading edge of the disk. Contrary, the wake behind square plates appears to be more uniform with no vortical structure shed off from the main turbulent wash.

Introduction

Understanding the physical mechanisms involved in the free fall of particles in viscous media has been the focus of many studies across a broad range of disciplines, from earth science to engineering problems. Examples of these phenomena in natural environments include seed dispersal, Sabban & van Hout (2011), the deposition of volcanic ash, Wilson & Huang (1979), the falling of rain droplets and ice crystals, List & Schemenauer (1971), Jayaweera (1972), Kajikawa (1992), and sedimentation processes Feng *et al.* (1994). Fundamental research of free falling particles have focused on the wake structure, vortex shedding mechanisms and body-to-fluid interactions with the objective of understanding the characteristics of the paths of the falling objects and controlling dispersion among other phenomena.

Dye visualisation was firstly used by Willmarth *et al.* (1964) to get insight into the wakes of falling axisymmetric bodies in a liquid media. Posterior studies focused on the wake structure of free falling and rising axisymmetric bodies; being the wake of thin disks with several aspect ratios a topic of discussion, Auguste & Fabre (2010), Zhong & Lee (2012), Bobinski *et al.* (2014). Like any body falling in a viscous medium, disks exhibit distinctive trajectories and vortex shedding mechanisms.

In the limit of small thickness-to-width ratio, the falling regime of disks and plates can be predicted once the Reynolds number and the dimensionless moment of inertia are known. The first phase diagram, experimentally defined for disks by Willmarth *et al.* (1964), mapped three different falling regimes; i.e steady, fluttering and tumbling. Following the same approach, Smith (1971) constructed the corresponding phase diagram for 2-Dimensional falling plates. The original phase diagram defined by Willmarth *et al.* (1964) has undergone several adaptations, being the most relevant the definition of the chaotic regime by Field *et al.* (1977) and the sub-regimes found by Lee *et al.* (2013) within the periodic fall.

Although their geometry is of interest to many natural processes such as seed dispersal and meteorology, other planar particles than disks have received notably less attention. Early investigations on the steady fall of planar crystals by List & Schemenauer (1971) showed that the drag coefficient evolution with Reynolds number (for $Re < 100$) for snow crystal models was an almost parallel curve to the one for disks; as the cross-sectional area of the models decreased the drag coefficient increased. They also observed that by $Re \approx 200$ small oscillations were present in disks, hexagonal plates and broad-branched models, with the strongest oscillations in disks. Jayaweera (1972) also studied the steady free fall of several planar particles and showed that the terminal velocity of star-shape particles was up to 25% smaller than the one for the equivalent disk. Recent wind tunnel experiments by Nedic *et al.* (2013) focused on turbulent flow past fractal plates and showed the existence of axisymmetric wakes behind this 'high-drag' wake generators. However, a gap still remains on how the wake instabilities arise in the case free falling planar particles.

Here, we describe and compare the motion of a free falling disk with a square planar particle, both of them with nearly the same Reynolds number and similar moment of inertia. The surrounding flow is also investigated by means of volumetric velocimetry so that the coupling between vortex shedding and particle motion can be addressed. This study is focused on the stage where terminal velocity has been reached.

Experimental setup

The experiments were conducted in a 0.5-m-high open tank with a rectangular cross section of 0.8-m-long and 0.45-m-wide. Particles used in this study are manufactured to have the same frontal area within the precision of the laser cutter $\pm 0.5mm$, as seen in Table 1. A set of drops for each particle is performed in water at room temperature, $\rho_f = 0.998 g/cm^3$ and $\nu = 1.004 \cdot 10^6 Ns/m^2$. The water media is seeded with 55 μm polycrystalline particles.

The particles are released from a distance of approximately two disk diameters below the top surface so that entry and surface effects

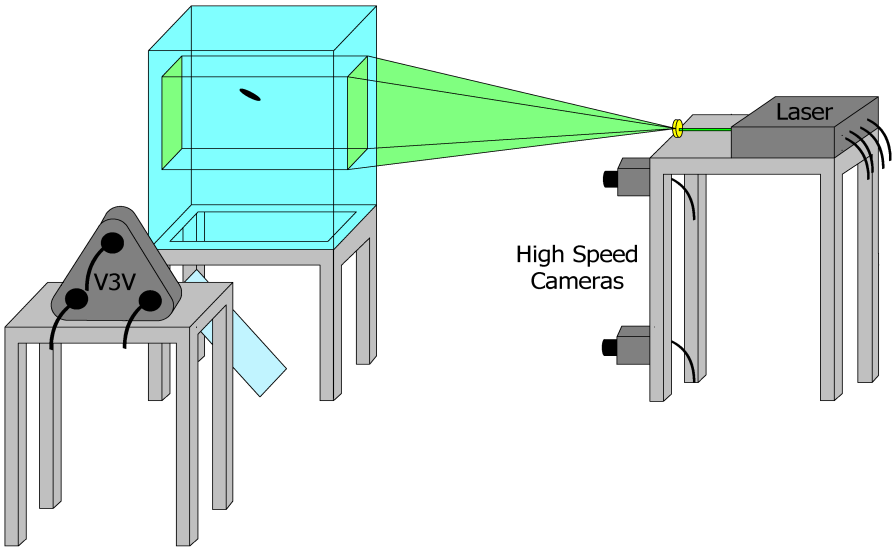

Figure 1. Sketch of the experimental setup.

Table 1. Characteristics of the particles geometry, mean descent velocity ($\langle V_z \rangle$) and velocity standard deviation (σ_{V_z}).

	Disk	Square
$A_p(cm^2)$	4.34	4.41
$Mass(g)$	1.07	1
$\langle V_z \rangle (mm \cdot s^{-1})$	58 ± 2	55 ± 3
σ_{V_z}	32	23

are avoided. The drop position is cantered to avoid wall effects during the particle fall and the particles are released horizontal with zero initial velocity. The particles used are made of acrylic with a density ratio $\rho_p/\rho_f = 1.2$, frontal area $A_p \approx 4.4cm^2$ and thickness $t = 0.2cm$, all particles are painted in black for image processing. All particles are held in their initial position by a suction cup smaller than their internal diameter. The suction cup was part of a rigid structure, attached to the water tank.

Two cameras were used to capture two views of the falling particle. One camera is used in conjunction with a mirror to capture the bottom view of the particle motion, $(X-Y)$ coordinates, while the other camera records the descent motion of the particle (Z) coordinate. The cameras are both focussed on the midpoint of the tank to minimise the lens curvature distortion. The trajectories are recorded at 7.25 frames per second to be synchronised with the V3V system. In each frame the dark particle projection is recorded on the white background and the position of the particle centre of mass is obtained by locating the geometric centre of each particle projection.

A set of releases for a sphere falling in air is performed. These trajectories helped establishing limitations on the accuracy associated with the drop mechanism as well as the measurements taken by the cameras and account for image distortion from the lens. The variance in the landing position is interpreted as the uncertainty of the system, being two to three orders of magnitude smaller than the sphere diameter. This is in accordance with the uncertainty typically found in the literature Heisinger *et al.* (2014).

The process followed to obtain the particle centre of mass does not add any uncertainty for the case of a thin disk or any planar particle with an even number of sides. The transition from the initial condition to the steady motion is not the objective of this study; therefore, the trajectories are studied after the particle reached a steady fluttering state. A distance of 7 disk diameters from the mechanism is considered to be enough and the particle position at that height is recorded as the origin of the trajectory. Before each drop, the fluid was checked to be quiescent. This was achieved by visualising tracer particles with a 4MP camera. The particles were realised from the full rest state by opening a T-valve to atmospheric pressure on the vacuum circuit.

Three-dimensional measurements of the instantaneous velocity field in the vicinity of the particles were obtained with a V3V system from TSI. Three 4MP (2048 x 2048 pixels), 12-bit frame-straddle CCD cameras were aligned in a coplanar triangle pattern to map a field of view (FOV) of 140 mm x 140 mm x 60 mm, as seen in figure 1. A synchroniser by TSI was used as an external trigger and connected to the laser and the camera system. A 200 mJ/pulse double-pulsed laser (Litron) was used to illuminate the FOV. The two-frame double expose was set at a 7.25 Hz and image triplets were analysed via Insight 4G software from TSI. A 75% of node volume overlap in the velocity interpolation process was defined, resulting in a vector grid spacing of $2.5mm$. Here, the particles were released above the FOV to assure the capture of 'periodic' fluttering. For each particle, 10 drops were collected, fully processed and reviewed to assure the robustness of the results.

Determination of non-dimensional parameters

There are six dimensional quantities that characterise the motion of a freely falling disk in a viscous media; the characteristic length, the thickness and the density of the disk, the density and kinematic viscosity of the fluid and the acceleration due to gravity. Since the thickness to length of the particle is very small ($\beta < 0.1$) the dynamics of the fall is independent of this parameter and therefore, the Reynolds number (Re) and the dimensionless moment of inertia (I^*) are the two non-dimensional numbers that define the motion of the disk.

The dimensionless moment of inertia of a disk was defined by Willmarth *et al.* (1964) as $I^* = \frac{I_p}{\rho_f d^5}$. However, this definition can not be easily adapted to particles with other frontal geometries. It is for this reason that we re-define the non-dimensional inertia by

changing the disk diameter for a length-scale (L) that can be used in conjunction with other geometries, being $L = \sqrt{A_p}$. Doing so, the dimensionless moment of inertia is re-defined as,

$$I^* = \frac{I_p}{\rho_f L^5} \tag{1}$$

This new approach present in here allows the direct comparison not only of particles with different frontal area but with severe differences in frontal geometry.

To be consistent with the definition proposed for the dimensionless moment of inertia, the Reynolds number is estimated using also this characteristic length (L) and the mean descent velocity ($\langle V_z \rangle$). Therefore,

$$Re = \frac{L\langle V_z \rangle}{\nu} \tag{2}$$

Since the characteristic length of the reference sphere used to non-dimensionalized the inertia of the particle has changed from d to $\sqrt{A_p}$ the regime map for disks in the (Re, I^*) domain has to be modified accordingly. Figure 2 shows the regime map defined by Field *et al.* (1977) but re-scaled for the new definition of the dimensionless moment of inertia and the Reynolds number based on L. The Reynolds number and dimensionless moment of inertia for disks and squares studied in here appear to be both within the fluttering regime originally defined by Field *et al.* (1977).

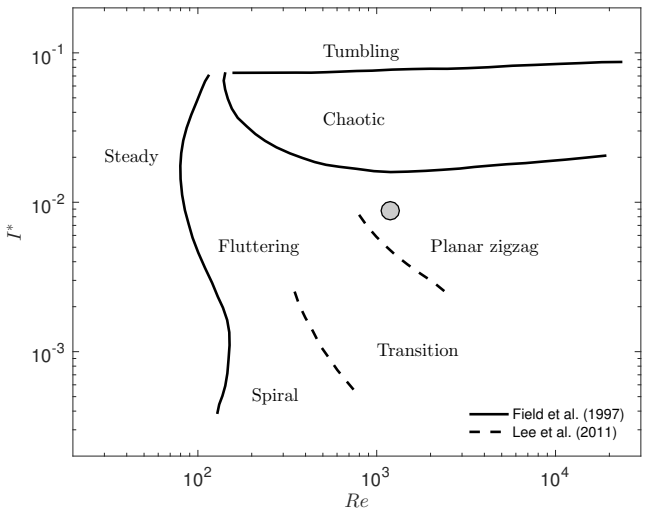

Figure 2. Modified $Re - I^*$ phase diagram for thin circular disks. The circle corresponds to the region of the present work. ($Re \approx 1200, I^* \approx 9 \cdot 10^3$).

Results

In this section results on the trajectory characteristics and flow visualisation of the wake behind of the disks and the square plate are presented. First, an introduction to the trajectory characteristics obtained from the high speed cameras is carried out and the differences between both geometries are compared. Second, the vorticity present in the wake of the particles is shown for trajectories that are representative of the motion of each geometry.

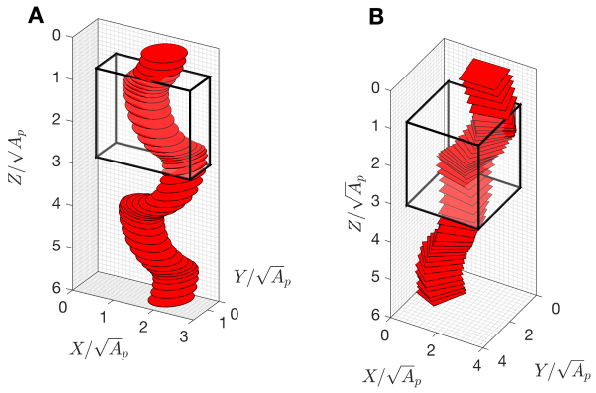

Figure 3. Reconstructed trajectory of a falling disk (A) and a square plate (B). The 3D box shows the region where the volumetric velocimetry was performed.

Trajectory Characteristics

Two views of the particle descent are used to acquire synchronously the 3D position of the particle. Central difference derivation was used to obtain velocities with respect to the global coordinate system. The first trajectory feature of interest is the

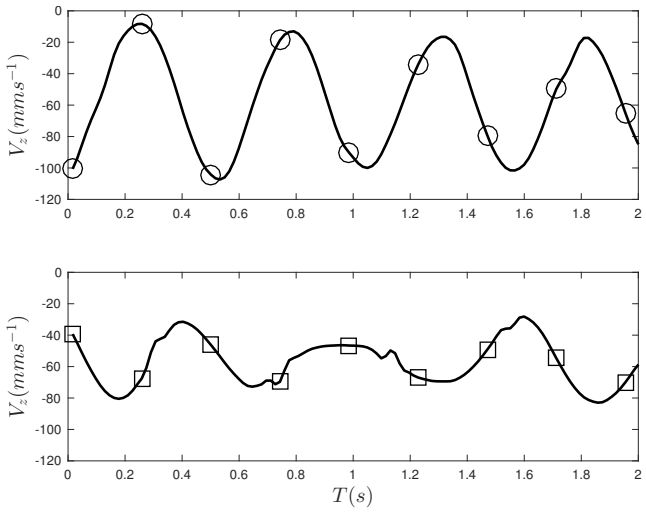

Figure 4. Measured descent velocity for a characteristic trajectory of a disks and a square plate.

mean terminal velocity. The magnitude of the descent velocity for disks and square plates is consistent with the results found in Jayaweera (1972); List & Schemenauer (1971); Kajikawa (1992) for planar crystal-like particles, where the descent velocity reduced as the perimeter increased. However, the Reynolds number investigated in here is an order of magnitude higher than the range investigated in the literature and therefore direct quantitative comparison is inappropriate. The descent velocity along the trajectory is obtained from each pair of successive particle positions, so that the standard deviation of the descent velocity is obtained as the velocity fluctuation along single trajectories. Square plates show a velocity standard deviation about 30% smaller than disks, so that the descent motion of these particle is much steadier than the observed in disks.

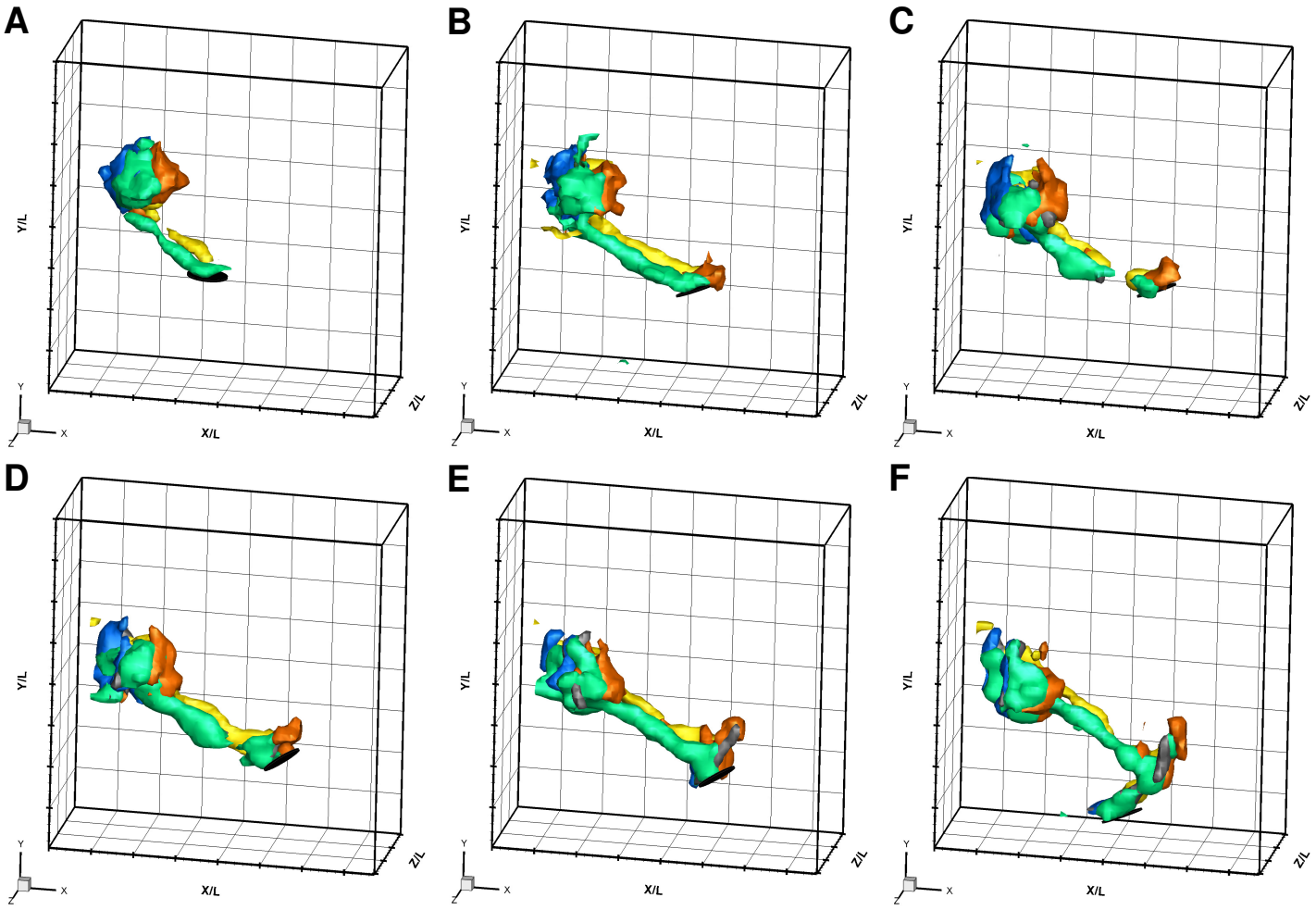

Figure 5. Instantaneous iso-surfaces of vorticity magnitude for a free falling disk describing a 'Quasi-Planar' motion. The elapse time between subsequent images is $\Delta t = 0.35s$. The iso-surfaces have constant amplitude of $1.5s^{-1}$. The vortical structures present in the wake of the disk are shown to be quasi-symmetric with respect to the vertical plane that contains the trajectory motion. Blue and orange represent positive and negative Z-vorticity, green and yellow X-vorticity and black and grey Y-vorticity.

Table 2. Values of mean ($\langle V_z \rangle$) and standard deviation (σ_{V_z}) of the fall velocity. Particle Reynolds number (Re_p) is based on the mean fall velocity and the characateristic length-scale previously defined (L).

	Disk	Square
Re	1247	1183
I^*	$8.7 \cdot 10^{-3}$	$9.5 \cdot 10^{-3}$

The difference in the trajectory characteristics can be seen also in the frequency content of the descent velocity, disks show a dominant frequency $f \approx 1.8Hz$, while the frequency content for square plates does not have such a characteristic frequency due to its much uniform descent. The Strouhal number, defined as $St = f\sqrt{A_p}/V_z$, is estimated to compare the oscillating flow mechanism along the particle descent for disks. In here, $St \approx 0.65$ which is in in good agreement with the Strouhal number found for disks in Lee *et al.* (2013).

The strong differences in the falling dynamics between different particles is therefore investigated by means of volumetric flow visualisation as explained in the previous section.

Wake Characteristics.

The effect of vorticity in the flow behind the particle is one of the key features to understand the path instability of planar particles. Disks freely falling and describing Quasi-Planar trajectories have been extensively investigated during the last 60 years (Willmarth *et al.* (1964), Stringham *et al.* (1969), Field *et al.* (1977), Fernandes *et al.* (2007), Lee *et al.* (2013)). Some of them include qualitative visualisations of the wake as in Fernandes *et al.* (2007) and quantitative planar image velocimetry as in Lee *et al.* (2013). Fernandes *et al.* (2005) showed that the phase difference between the velocity and the inclination of the body axis greatly differs for the irrotational theory estimation so that vortical effects present in the wake were shown to be crucial in the body dynamics.

Disks

The wake behind a disk describing 'Quasi-Planar' motion shows the strong differences in the dynamics of the trajectory sections previously reported. As the disk describes a gliding section of the trajectory, a significant stream-wise vorticity structure progressively form in the downstream direction from both sides of the disk. This vortical structure is a pair of counter-rotating vortices (with its main

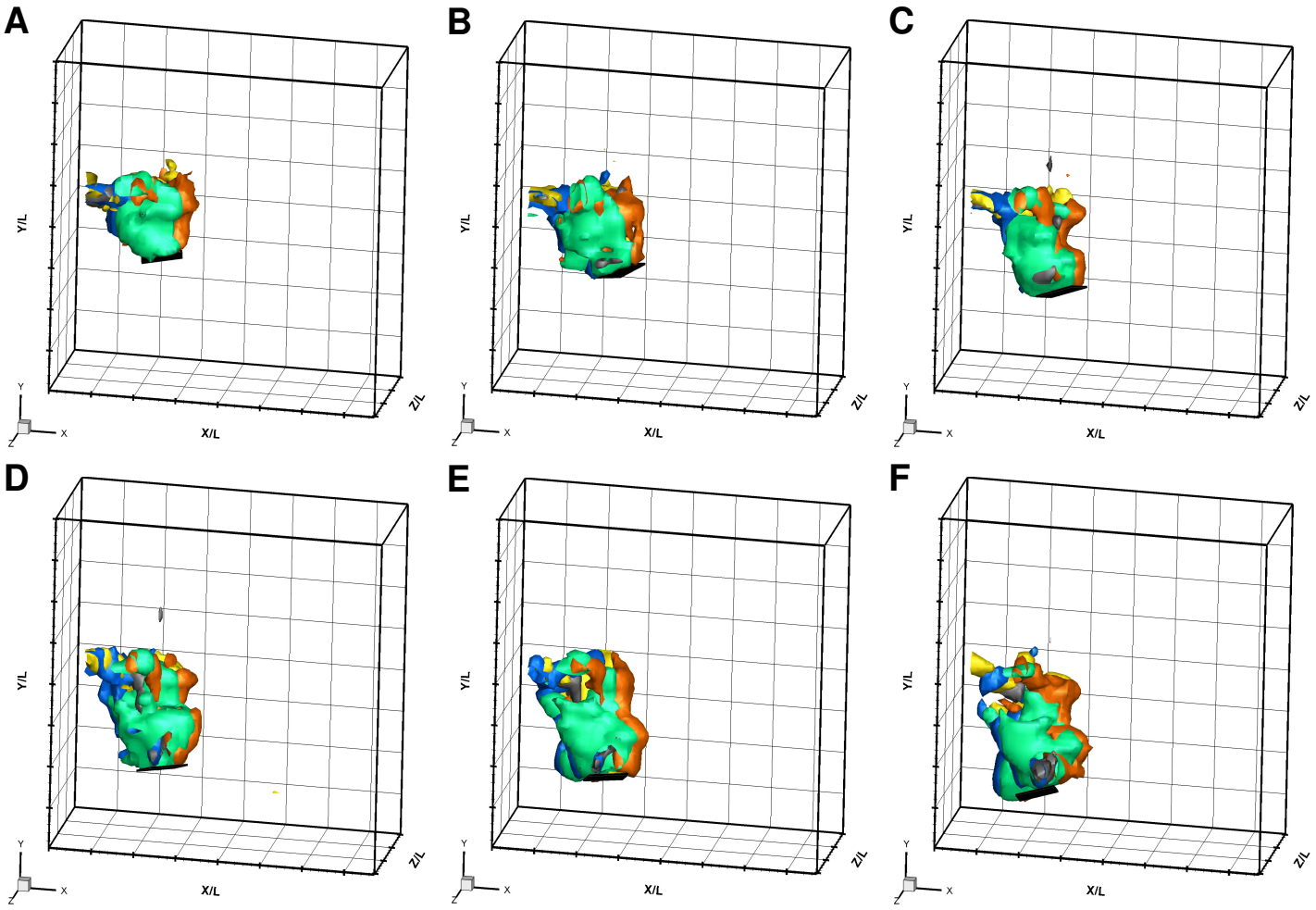

Figure 6. Instantaneous iso-surfaces of vorticity magnitude for a free falling square plate describing a 'Highly 3D' motion. The elapse time between subsequent images is $\Delta t = 0.35s$. The iso-surfaces have constant amplitude of $1.5s^{-1}$. Blue and orange represent positive and negative Z-vorticity, green and yellow X-vorticity and black and grey Y-vorticity.

vorticity component align with the motion of the disk), as shown in fig. 5. This vortical structure adds to the vorticity formed during the turning section (with its main vorticity component normal to the plane of motion), creating a hairpin vortex that is shed into the wake. Once the vortex is released downstream, there is a period of time during which the wake-induced torque is almost zero and the torque balance is momentarily controlled by purely inertial effects, as reported in Lee *et al.* (2013).

It is at this point when the disk-to-fluid relative inertia controls the subsequent possible scenarios. For the case of low dimensionless inertia (the case present in here), fluid inertia is dominant and therefore the torque balance is controlled by the added-mass contribution, realigning the disk axis with its instantaneous velocity. Thus, the disk transverse velocity reduces to zero and the disk describe a new cycle, following a Quasi-planar motion. The dominant vortical structures induced by the disks are shown and linked to their motion in figure 5. Figure 5 shows a set of images of the disk oscillatory motion together with iso-surfaces of vorticity magnitude. Instantaneous images are $1/7.25s$ apart from each other, and the first image corresponds to $\Delta t = 2s$ after the drop of the disk.

The vortex ring shed off at every extreme point of the oscillatory motion is responsible for the regions of strong downwash in the wake of the disk. The magnitude of the velocity in the region dominated by the downwash is of the same order of magnitude of the maximum descent velocity observed along the disk trajectory.

Square Plates

The wake behind a square plate shows a vortical structure much more uniform along the particle trajectory. The vortex structures are significantly different from those observed in the planar motion addressed in the previous section. Here, vorticity structures with different dominant vorticity components are formed indistinctly during the descent of the particle. Despite of the wake homogeneity during the particle fall, the fact that the square lacks axi-symmetry is responsible of differences in the wake region near the particle surface. These differences depend on the geometry of the instantaneous leading edge. Thus, when the square describes a section of the trajectory with any of its corners aligned with the direction of motion, a pair of counter-rotating vortices forms from both sides of the corners propagating downstream. However, the strong instabilities present in the particle wake quickly realign the particle to a different orientation and therefore the wake structure also changes. Instantaneous images are $1/7.25s$ apart from each other, and the first image corresponds to $\Delta t = 2s$ after the drop of the square plate.

Conclusion

We proposed a new definition for the non-dimensional inertia of the particle based on the particle frontal area and we investigated the effect of changing the particle frontal area on the particle dynamics and wake characteristics.

The trajectories for disks and squares exhibit some remarkable differences: the disks in the regime studied fall in a 'Quasi-planar' regime, while square plates show a trajectory with severe out-of-plane motion.

Three-dimensional measurements of the instantaneous velocity field showed the existence of two different phases in the periodic motion of a falling disk. First, near the extreme of the oscillatory motion the body rotation becomes large and hairpin vortices are formed and later shed off to the wake. Second, between the extremes of each cycle the disk described a gliding motion where a counter-rotating vortex pair developed on both side of the disks. A strong downwash region in the wake is localised in the vicinity of the hairpin vortices, inducing a flow velocity of the same order of magnitude than the maximum descent velocity seen along the disk trajectory. Contrary, the more uniform character of the trajectory of the square creates a more complex wake where the dominant turbulent scales appear to be quasi-independent of the particle orientation. This type of wake structure is similar to the one observed for disk describing spiral motion using dye visualisation in Lee *et al.* (2013).

In Lee *et al.* (2013), they described how a non-uniform lift distribution over the disk surface can create a lift-induced torque, leading to the disruption of the original planar motion. Following the same reasoning they showed how the non-dimensional inertia of the particle (I^*) might either stabilise or destabilise the system. Therefore, if $I^* < I^*_{crit}$ the system instabilities grow at every turning point, while if $I^* > I^*_{crit}$ the system becomes more stable. This non-uniform lift distribution explained in Lee *et al.* (2013) occurs naturally for particles with non-axisymmetric frontal geometries, fact that could explain why square plates with an even greater non-dimensional inertia do not show periodicity in their fall.

Acknowledgements

We thank Dr. M. Hyde for his helpful assistance with the V3V sytem. This work was supported by Aquavitrum Ltd., the Leverhulme Trust and the Faculty of Engineering and the Environment of University of Southampton.

REFERENCES

Auguste, F. & Fabre, D. Magnaudet, J. 2010 Bifurcations in the wake of a thick circular disk. *Theor. Compt. Fluid Dyn* **24**, 305–313.

Bobinski, T., Goujon-Durand, S. & Wesfreid, J. E. 2014 Instabilities in the wake of a circular disk. *Phys. Rev. E* **89**, 053–021.

Feng, J., Hu, H. H. & Joseph, D. D. 1994 Direct simulation of initial value problems for the motion of solid bodies in a newtonian fluid. part 1. sedimentation. *J. Fluid Mech* **261**, 95–134.

Fernandes, P.C., Ern, P., Risso, F. & Maugnadet, J. 2005 On the zigzag dynamics of freely moving axisymmetric bodies. *Phys. Fluids* **17**, 098107.

Fernandes, P.C., Ern, P., Risso, F. & Maugnadet, J. 2007 Dynamics of axisymmetric bodies rising along a zigzag path. *J. Fluid Mech* **606**, 209–223.

Field, S. B., Klaus, M., Moore, M. G. & Nori, F. 1977 Chaotic dynamics of falling disks. *Nature* **388**, 252–254.

Heisinger, L., Newton, P. & Kanso, E. 2014 Coins falling in water. *J. Fluid Mech.* **714**, 243–253.

Howe, M. 1995 On the force and moment on a body in an incompressible fluid, with application to rigid bodies and bubbles at low and high reynolds numbers. *Q. J. Mech. Appl. Maths* **48**, 401–426.

Jayaweera, K. O. L. F 1972 An equivalent disc for calculating the terminal velocities of plate-like ice crystals. *J. Atmos. Sci.* **29**, 596–597.

Kajikawa, M. 1992 Observations of the falling motion of plate-like crystals. part i: The free-fall patterns and velocity variations of unrimed crystals. *J. Meteor. Soc. Japan* **70**, 1–9.

Lee, C., Su, Z., Zhong, H., Chen, S., Zhou, M. & Wu, J. 2013 Experimental investigation of freely falling thin disks. part 2. transition of three-dimensional motion from zigzag to spiral. *J. Fluid Mech.* **42**, 77–104.

List, R. & Schemenauer, R. S. 1971 Free-fall behaviour of planar snow crystals, conical graupel and small hail. *J. Atmos. Sci.* **28**, 110–115.

Mougin, G. & Magnaudet, J. 2002 The generalized kirchhoff equations and their application to the interaction between a rigid body and an arbitrary time-dependent viscous flow. *Intl J. Multiphase Flow* **28**, 1837–1851.

Nedic, J., Vassilicos, J. C. & Ganapathisubramani, B. 2013 Axisymmetric turbulent wakes with new nonequilibrium similarity scalings. *Phys. Rev. Letters* **111**, 144503.

Sabban, L. & van Hout, R. 2011 Measurements of pollen grain dispersal in still air and stationary near homogeneous, isotropic turbulence. *J. Aerosol Science.* **42**, 867–882.

Smith, E. H. 1971 Autorotating wings: an experimental investigation. *J. Fluid Mech* **50**, 513–534.

Stringham, G. E., Simons, D. B. & Guy, H. P. 1969 The behaviour of large particles falling in quiescent liquids. *U.S. Department of Interior* .

Willmarth, W. W., Hawk, N. E. & Harvey, R. L. 1964 Steady and unsteady motions and wakes of freely falling disks. *Phys. Fluids* **7**, 197–208.

Wilson, L. & Huang, T. C. 1979 The influence of shape on the atmospheric settling velocity of volcanic ash particles. *Earth Planet Sci Lett* **44**, 311–324.

Zhong, H. J. & Lee, C. B. 2012 The wake of falling disks at low reynolds numbers. *Acta Mech. Sinica* **28**, 367–371.